Voltage-gated K^+ channels in layer 5 neocortical pyramidal neurones from young rats: subtypes and gradients

Alon Korngreen and Bert Sakmann

Abteilung Zellphysiologie, Max-Planck-Institut für Medizinische Forschung, Jahnstrasse 29, D-69120 Heidelberg, Germany

(Received 21 January 2000; accepted after revision 9 March 2000)

1. We investigated the types and distribution of voltage-gated K^+ channels in the soma and apical dendrite of layer 5 (L5) neocortical pyramidal neurones, of young rats (postnatal days 13–15), in acute brain slices.

2. A slow inactivating outward K^+ current and a fast inactivating outward K^+ current were detected in nucleated patches. The slow K^+ current was completely blocked by tetraethylammonium (TEA) with an IC_{50} of 5 ± 1 mM (mean ± S.E.M.) and was partially blocked by 4-aminopyridine (4-AP). The fast K^+ current was blocked by 4-AP with an IC_{50} of $4{\cdot}2 \pm 0{\cdot}5$ mM, but was not blocked by TEA.

3. The activation kinetics of the slow K^+ current were described by a second order Hodgkin-Huxley model. The slow K^+ current displayed bi-exponential inactivation. A fourth order Hodgkin-Huxley model for activation and first order for inactivation described the kinetics of the fast K^+ current.

4. In somatic cell-attached recordings, three classes of single K^+ channels could be differentiated based on their unitary conductance and inactivation kinetics, a fast inactivating channel having a conductance of 13 ± 1 pS, a slow inactivating channel having a conductance of $9{\cdot}5 \pm 0{\cdot}5$ pS, and a very slowly inactivating channel having a conductance of 16 ± 1 pS.

5. The inactivation time constants of the slow and of the very slow K^+ channel corresponded to the two inactivation time constants of the slow K^+ current observed in nucleated patches. This suggested that two distinct K^+ channels mediated the slow K^+ current in nucleated patches.

6. The three subtypes of K^+ channels that were observed in somatic recordings were present along the apical dendrite. The amplitude of ensemble K^+ currents in cell-attached patches decreased along the apical dendrite as the distance from the soma increased, with a slope of $-0{\cdot}9 \pm 0{\cdot}3$ pA per 100 μm.

7. The results suggest that the decrease of the voltage-gated K^+ channel density from the soma along the apical dendrite of L5 pyramidal neurones helps to define a distal, low threshold region for the initiation of dendritic regenerative potentials.

Pyramidal neurones of layer 5 in the neocortex are primary output cells of the cortex (White, 1989). They have an elaborate dendritic tree that contains several types of voltage-gated channels such as Na^+, K^+ and Ca^{2+} channels. These channels take part in the spread of both subthreshold (Markram & Sakmann, 1994; Magee *et al.* 1995; Magee & Johnston, 1995; Koester & Sakmann, 1998) and propagation of suprathreshold (Turner *et al.* 1991; Amitai *et al.* 1993; Markram & Sakmann, 1994; Stuart & Sakmann, 1994; Schiller *et al.* 1995, 1997; Spruston *et al.* 1995; Stuart *et al.* 1997*a*; Larkum *et al.* 1999) regenerative potentials in dendrites. Following suprathreshold stimulation axonally initiated action potentials propagate back into the dendritic arbor (Stuart & Sakmann, 1994).

The types, kinetics, spatial distribution and second messenger modulation of voltage-gated channels found in the soma and dendrites determine the properties of the back-propagating action potential (Nicoll, 1988; Yuste & Tank, 1996; Stuart *et al.* 1997*b*; Tsubokawa & Ross, 1997). Voltage-gated K^+ channels regulate, among other properties, the rate of repolarisation, the level of after-hyperpolarisation and the firing frequency of the neurone (Llinás, 1988). Of the voltage-gated channels found in neurones, K^+ channels are the most diversified (Jan & Jan, 1997). Due to this diversity, it is almost impossible to understand *a priori* the electrophysiology of a given neurone without a detailed study of the K^+ channel types it expresses.

Recently it has been shown for pyramidal neurones of the CA1 region in the hippocampus that the density of a fast K^+ current increased with distance from the soma along the apical dendrites (Hoffman *et al.* 1997). This inhomogeneous distribution caused a marked attenuation in the amplitude of the back-propagating action potential, highlighting the need for detailed knowledge of the spatial distribution of voltage-gated K^+ channels in dendrites. In L5 neocortical pyramidal neurones the types, distribution and functions of voltage-gated K^+ channels are less characterised, although K^+ channels were detected in recordings from somatic cell-attached patches (Kang *et al.* 2000) and apical dendrites of these neurones (Stuart *et al.* 1993; Bekkers & Stuart, 1998). Furthermore, bath application of the K^+ channel blocker TEA increased the Ca^{2+} influx, induced by a back-propagating action potential, measured in the apical dendrite (Markram *et al.* 1995).

The goal of the present study was to investigate the types and distribution of voltage-gated K^+ channels in L5 neocortical pyramidal neurones. For this, we determined the subtypes, pharmacological properties, and kinetics of voltage-gated K^+ channels in nucleated patches from the soma of L5 pyramidal neurones. The K^+ channel density in the soma and apical dendrite was characterised by making cell-attached recordings up to a distance of 430 μm from the soma. Part of this work appeared in abstract form (Korngreen *et al.* 1999).

METHODS

Slice preparation

Slices (sagittal, 300 μm thick) were prepared from the somatosensory cortex of 13- to 15-day-old Wistar rats that were killed by rapid decapitation using previously described techniques (Stuart *et al.* 1993). Slices were perfused throughout the experiment with an oxygenated artificial cerebrospinal fluid (ACSF) containing (mM): 125 NaCl, 25 $NaHCO_3$, 2·5 KCl, 1·25 NaH_2PO_4, 1 $MgCl_2$, 2 $CaCl_2$, 25 glucose (pH 7·4 with 5% CO_2, 310 mosmol kg^{-1}). All experiments were carried out at room temperature (20–22 °C). Pyramidal neurones from L5 in the somatosensory cortex were visually identified using infrared differential interference contrast (IR-DIC) videomicroscopy (Stuart *et al.* 1993).

Solutions and drugs

The standard pipette solution contained (mM): 125 potassium gluconate, 20 KCl, 10 Hepes, 4 MgATP, 10 sodium phosphocreatine, 0·5 EGTA, 0·3 GTP (pH 7·2 with KOH, 312 mosmol kg^{-1}). For cell-attached recordings the pipette solution contained (mM): 135 NaCl, 5·4 KCl, 1 $MgCl_2$, 1·8 $CaCl_2$, 5 Hepes, 100 nM TTX (pH = 7·2 with NaOH, 290 mosmol kg^{-1}). 4-Aminopyridine (4-AP) (Merck) was first dissolved in doubly distilled water and pH corrected with HCl to 7·4 prior to addition to the bath solution. In experiments with high concentrations of TEA or 4-AP (more than 3 mM) the equivalent amount of NaCl was removed from the bath solution. Tetrodotoxin (TTX, Tocris, Bristol, UK), dendrotoxin-I (DTX-I), MCD-peptide (MCD-P), tityustoxin Kα (TsTx-Kα), margatoxin (MgTx), stychodactyla toxin (ShTx) (Peptide Institute, Japan), BDS-I and agitoxin (AgTx) (Alomone Labs, Jerusalem, Israel) were stored at −20 °C as stock solutions in doubly distilled water. The toxins were applied locally using theta tubing that was coated with silicone using Sigmacote (Sigma). The $NaHCO_3$ in the bath solution was replaced with Hepes for the experiments in which toxins were used and 0·1 mg ml^{-1} cytochrome C was added to the solution to prevent non-specific binding.

Nucleated outside-out patches

Nucleated outside-out patches (Sather *et al.* 1992) were extracted from the soma of L5 pyramidal neurones. Briefly, negative pressure (18–23 kPa) was applied when recording in the whole cell configuration, and the pipette was slowly retracted. Provided that the retraction was gentle it was possible to obtain large patches of membrane engulfing the nucleus of the neurone. Following the extraction of the patch the pressure was reduced to 4–10 kPa for the duration of the experiment. All measurements from nucleated and cell-attached patches were carried out with the Axopatch-200B (Axon Instruments) amplifier. The capacitative compensation circuit of the amplifier was used to reduce capacitative transients. Nucleated patches were held at −50 mV unless stated otherwise. Linear leak and capacitative currents were subtracted off-line by the scaling of 20–30 average pulses taken at hyperpolarised voltages (−80 to −100 mV). Currents were filtered with 2–10 kHz and sampled at rates 2–10 times higher than the filtering frequency.

The surface area of nucleated patches was estimated visually from video images. The surface area of the patch, calculated from the area of the focused image, was 440 ± 10 μm^2 ($n = 30$). The average series resistance, input resistance, and capacitance were $13{\cdot}2 \pm 0{\cdot}7$ MΩ ($n = 82$), $2{\cdot}7 \pm 0{\cdot}2$ GΩ ($n = 66$) and $2{\cdot}2 \pm 0{\cdot}1$ pF ($n = 82$), respectively. The reference electrode was an Ag–AgCl pellet placed in pipette solution and connected by way of an agar bridge containing 150 mM KCl to the experimental chamber. Under these conditions the total voltage offset due to electrode and liquid junction potentials (Neher, 1992) was measured as 2 mV. Membrane potential was not corrected for this potential difference. Recordings were made with fire-polished Sylgard (General Electric, RTV615)-coated pipettes (5–8 MΩ).

Cell-attached recordings

Cell-attached recordings were made to establish the density of voltage-gated K^+ channels. It was important to control the area of the cell membrane sucked into the patch pipette. To reduce the variability two precautions were taken. The size of the pipettes and the sealing procedure were monitored. The average open tip resistance of the pipettes used to record from somatic and dendritic patches was $10{\cdot}3 \pm 2{\cdot}6$ MΩ (mean ± S.D.) and $10{\cdot}3 \pm 2{\cdot}5$ MΩ, respectively. In experiments designed to obtain recordings from a single channel, smaller pipettes were used (13 ± 3 MΩ). All pipettes were coated with Sylgard and fire polished before use. In an effort to obtain patches with similar area a constant experimental procedure was used. Positive pressure (2–4 kPa) was applied to the pipette as it was advanced to the cell. The tip of the pipette was gently pressed against the membrane and a negative pressure that did not exceed 1 kPa was applied. It has been shown that the area of the patch membrane was correlated to the conductance of the pipette (Sakmann & Neher, 1995). This made it possible to normalise currents to the size of the pipette, and thus to the area of the patch membrane. This normalisation was not applied here since some of the patches obtained did not contain any channels. In cell-attached experiments no agar bridge was used. As the pipette solution had a similar NaCl concentration to that of the bath solution the liquid junction potential was zero. Linear leak and capacitance currents were subtracted off-line from empty traces. Residual line frequency noise was removed with a Hum Bug noise eliminator (Quest Scientific, Vancouver, Canada). Occasional large brief noise spikes were visually identified and removed from the current traces.

Analysis

All off-line data analysis including curve fitting was carried out with programs in IGOR (WaveMetrics, Lake Oswego, USA) on a Macintosh computer. Experimental results were observed in cells from two or more animals. Therefore, all the results for a particular experiment were pooled and displayed as means ± S.E.M. Groups were compared with two-way ANOVA. Tests of correlation were performed with a Spearman rank order test using SigmaStat 1.1 (Jandel Scientific). Current traces were analysed assuming a Hodgkin-Huxley model (Hodgkin & Huxley, 1952). The activation and deactivation current traces were fitted to the general equation:

$$I(t) = (\sqrt[n]{I_\infty} - (\sqrt[n]{I_\infty} - \sqrt[n]{I_0})\exp(-t/\tau))^n, \quad (1)$$

where t is time, I_∞ is the steady-state current, I_0 is the current at $t = 0$, τ is the time constant of the exponential relaxation, and n is the number of gates in the model. Since I_0 is close to zero at the holding potential the above equation simplifies to:

$$I(t) = I_\infty(1 - \exp(-t/\tau))^n.$$

Correspondingly, tail currents were fitted to:

$$I(t) = I_0\exp(-nt/\tau).$$

The normalised conductance was fitted to a Boltzmann equation:

$$G/G_{max} = (1/\{1 + \exp(-(V - V_{½})/k)\})^n, \quad (2)$$

where G/G_{max} is the conductance normalised to its maximal value, V is membrane potential, $V_{½}$ is the voltage at which the conductance is half-maximal (for a single gate, $n = 1$), and k is the slope factor. To allow the comparison between $V_{½}$ and k values obtained in different sections of the paper the values are reported throughout the text for a fit to eqn (2) with one gate ($n = 1$). When the currents were analysed according to a higher order Hodgkin-Huxley model the results of the fit to eqn (2) with more gates are given in the figure legends.

RESULTS

Outward currents in nucleated patches

To isolate K^+ currents in nucleated patches, voltage-gated Na^+ channels were blocked by addition of 100 nM TTX to the bath solution. To measure the contribution of voltage-gated Ca^{2+} currents to the total current in the patch K^+ was replaced with Cs^+ in the pipette solution. The rundown of voltage-gated Ca^{2+} current in nucleated patches was rapid, and was usually complete within 1–2 min after patch isolation ($n = 3$, data not shown). Bath application of 50 μM $CdCl_2$, to block voltage-gated Ca^{2+} channels, did not change the magnitude or the time course of the outward current when K^+ was the major cation in the pipette solution ($n = 4$). This suggested that the contribution of a Ca^{2+}-activated K^+ current to the outward current in nucleated patches was negligible. In two patches that were hyperpolarised to −110 mV for 1 s a slowly activating inward current was observed that could have been a hyperpolarisation-activated current (I_h). The amplitude of these currents did not exceed 20 pA.

Kinetic separation of K^+ currents

Depolarising voltage steps, following a pre-pulse of 400 ms to −110 mV, evoked time- and voltage-dependent outward currents (Fig. 1*A*). The time course of the outward currents changed when a 60 ms voltage step to −50 mV was inserted after the −110 mV pre-pulse (Fig. 1*B*). Subtraction of the currents obtained by the two voltage protocols revealed a fast inactivating current (Fig. 1*C*). This 'difference' current decayed with a time constant of 8·2 ± 0·6 ms ($n = 5$) at +80 mV to a sustained current (Fig. 1*C*). When shorter pulses to −50 mV were used the peak amplitude of the difference current decreased. Longer pulses to −50 mV did not change the amplitude of the difference current. However, the amplitude of the sustained difference current increased (data not shown). This suggested that a 60 ms pre-pulse to −50 mV inactivated, in addition to a fast inactivating K^+ current, a current with slower inactivation kinetics. The difference current (Fig. 1*C*) will be referred to as the 'fast' K^+ current while the current remaining after the −50 mV pre-pulse (Fig. 1*B*) will be referred to as the 'slow' K^+ current.

The normalised average peak conductances, calculated by dividing the maximal current amplitude at each command voltage by the driving force calculated from the Nernst equation, were fitted to a Boltzmann function with one gate (Fig. 1*D*). The fit yielded $V_{½} = -3 \pm 1$ mV and $k = 10 \pm 1$ mV for the slow K^+ current (Fig. 1*D*, $n = 5$). The mean peak conductance was 2·9 ± 0·3 nS ($n = 5$), and the mean peak conductance density, estimated using the calculated membrane area of the patch, was 6·6 ± 0·7 pS μm^{-2}. The fit of the normalised average peak conductance of the fast K^+ current to a Boltzmann function gave $V_{½} = -3 \pm 1$ mV and $k = 20 \pm 2$ mV (Fig. 1*D*, $n = 5$). The mean peak conductance was 1·2 ± 0·2 nS ($n = 5$), and the mean peak conductance density was 2·7 ± 0·5 pS μm^{-2}.

The inactivation of the currents in nucleated patches was examined with voltage clamp protocols similar to those used to investigate the activation. The voltage was stepped to +80 mV following 15 s pre-pulses to potentials from −110 to 0 mV (Fig. 2*A*). Following the pulse to +80 mV the voltage was stepped to −100 mV for 1 s to allow K^+ channels to recover from inactivation. This sequence was then repeated with a 60 ms pulse to −50 mV inserted after the 15 s conditioning pulse to inactivate the fast K^+ current (Fig. 2*B*). The inactivation curve of the fast K^+ current (Fig. 2*D*) was calculated from the maximal difference current (Fig. 2*C*). The inactivation curve for the slow K^+ current was calculated from the maximal current measured at +80 mV after the −50 mV pulse (Fig. 2*B*). The curves were fitted to a Boltzmann function with one gate to obtain $V_{½} = -66 \pm 3$ mV and $k = -10 \pm 1$ mV for the fast K^+ current and $V_{½} = -51 \pm 4$ and $k = -12 \pm 2$ mV for the slow K^+ current ($n = 5$).

Pharmacological separation of K^+ currents

The kinetic separation suggested that two types of K^+ conductances contributed to the observed current in nucleated patches. It might be that one or several types of channels mediated either of these currents. To evaluate the number of conductances in nucleated patches and to provide

tools that may be used to probe these conductances in isolation, several K^+ channel blockers were tested.

Block of a slow K^+ current by TEA

The effect of the blockers on the two types of kinetically separated K^+ currents was investigated by a combined voltage protocol. The protocol is illustrated in Fig. 3*A* in which the effect of 10 mM external TEA was examined. Two voltage clamp protocols, similar to those described in Fig. 1, were performed before and after the application of TEA. Following a 400 ms pre-pulse to −110 mV the total outward current was measured by a step to +80 mV (Fig. 3*A*, top traces). This was then repeated with a 60 ms pulse to −50 mV inserted after the −110 mV pre-pulse to isolate the slow K^+ current (Fig. 3*A*, middle traces). The fast current is given, as in Fig. 1, by the difference between the currents recorded with the two protocols (Fig. 3*A*, bottom traces). This double pulse protocol revealed that 10 mM TEA reduced the amplitude of the slow K^+ current without significantly affecting that of the fast K^+ current (Fig. 3*A*, $n = 13$). TEA also did not significantly affect the amplitude of the fast K^+ current at concentrations of 30 ($n = 5$) and 60 mM ($n = 3$, Table 1). The time constant of inactivation at +80 mV of the fast K^+ current was 8·8 ± 0·7 ms at 10 mM TEA ($n = 7$) and 8·7 ± 0·5 ms at 30 mM TEA ($n = 6$). Both of these values were not significantly different from the time constant of inactivation obtained using the kinetic separation protocol ($P = 0{\cdot}5$, ANOVA, Table 2). The concentration yielding half the slow current amplitude observed under control conditions (IC_{50}) was 5 ± 1 mM TEA (Fig. 3*B*).

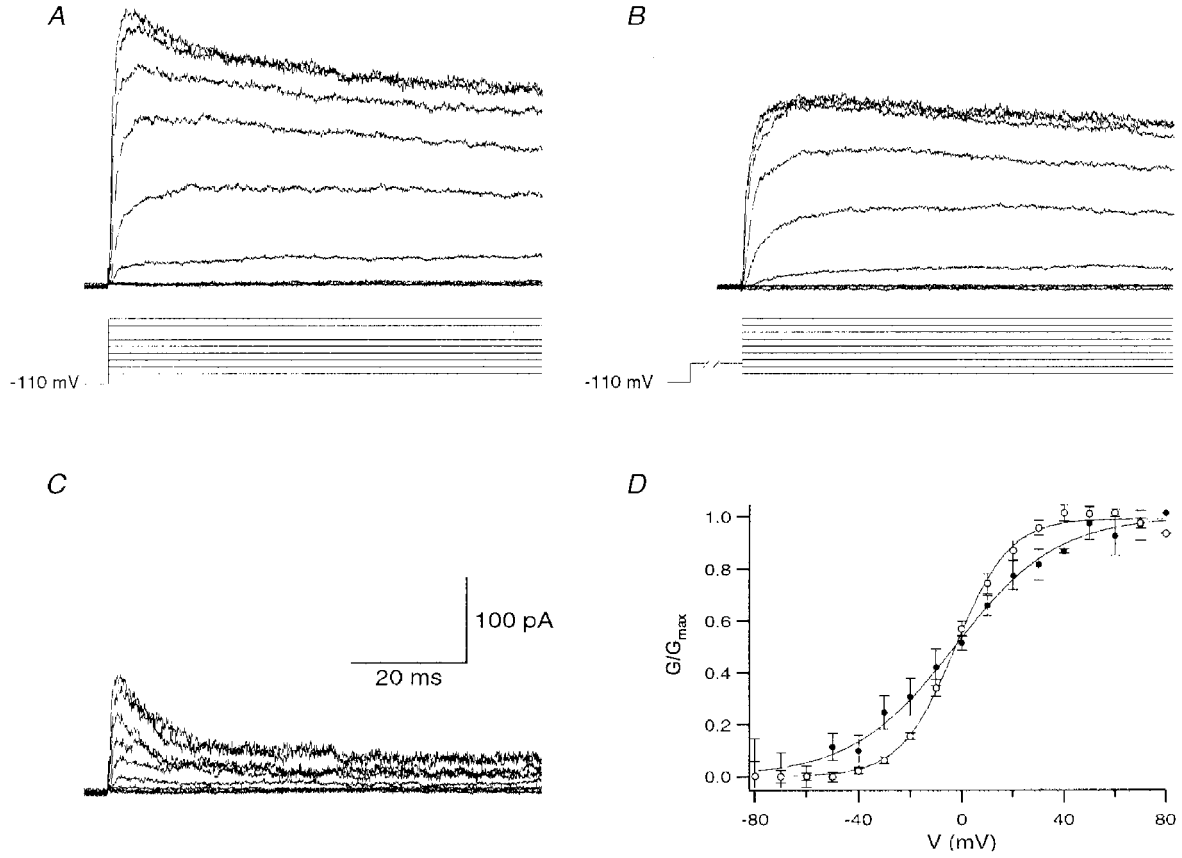

Figure 1. Kinetic separation of two types of voltage-gated K^+ currents in nucleated patches

A, outward currents recorded from a nucleated patch. The voltage protocol of a 400 ms pulse to −110 mV followed by a 90 ms pulse to voltages between −80 and +80 mV at 20 mV increments is shown below the current traces. The −110 mV pre-pulse was truncated to facilitate the display of the outward current. Sampled at 20 kHz and filtered at 5 kHz. Leak was subtracted off-line. *B*, outward currents from the same nucleated patch as in *A*. The voltage protocol was similar to that in *A* except for a 60 ms pulse to −50 mV inserted after the −110 mV step to inactivate the fast K^+ current. The voltage protocol is shown below the current traces. *C*, the difference current between the recording shown in *A* and that shown in *B*. The scale bars also apply to *A* and *B*. *D*, activation curves of the slow K^+ current isolated in *B* (○) and the fast K^+ current isolated in *C* (●). The conductance was calculated from the maximal current amplitude that was divided by the K^+ ion driving force calculated from the Nernst equation and normalised to the maximal conductance in a given series of voltages. The smooth lines are the fits to a Boltzmann function with one gate ($n = 5$). Error bars are ± S.E.M.

TEA (30 mM) did not affect the activation curve of the fast K^+ current (Fig. 4*A*). The values of $V_{½}$ (0 ± 1 mV) and k ($19 \pm 0{\cdot}7$ mV, $n = 11$, Boltzmann function with one gate) were not significantly different from those determined using the kinetic separation protocol ($P = 0{\cdot}1$ for $V_{½}$ and $P = 0{\cdot}55$ for k, ANOVA, Table 2). This lack of sensitivity of the fast K^+ current to TEA allowed us to further investigate the kinetics of this current. The kinetics were quantified by fitting the fast K^+ current to a Hodgkin-Huxley model. To increase the tail current amplitude the K^+ concentration in the ACSF was increased to 65 mM. This change in K^+ concentration did not change the activation or deactivation kinetics of the fast K^+ current ($n = 7$, data not shown). A Hodgkin-Huxley model with four activation gates (Fig. 4*B*) best described the activation and deactivation time course of

Table 1. TEA did not affect the peak amplitude of the fast K^+ current

[TEA] (mM)	I_{max}* (pA)	n
0	172 ± 21	5
10	180 ± 11 †	13
30	163 ± 17 †	11
60	203 ± 28 †	3

* The amplitude of the fast current was measured using the voltage protocol described in Fig. 3. † Not significantly different from the control value (ANOVA). Error is S.E.M.

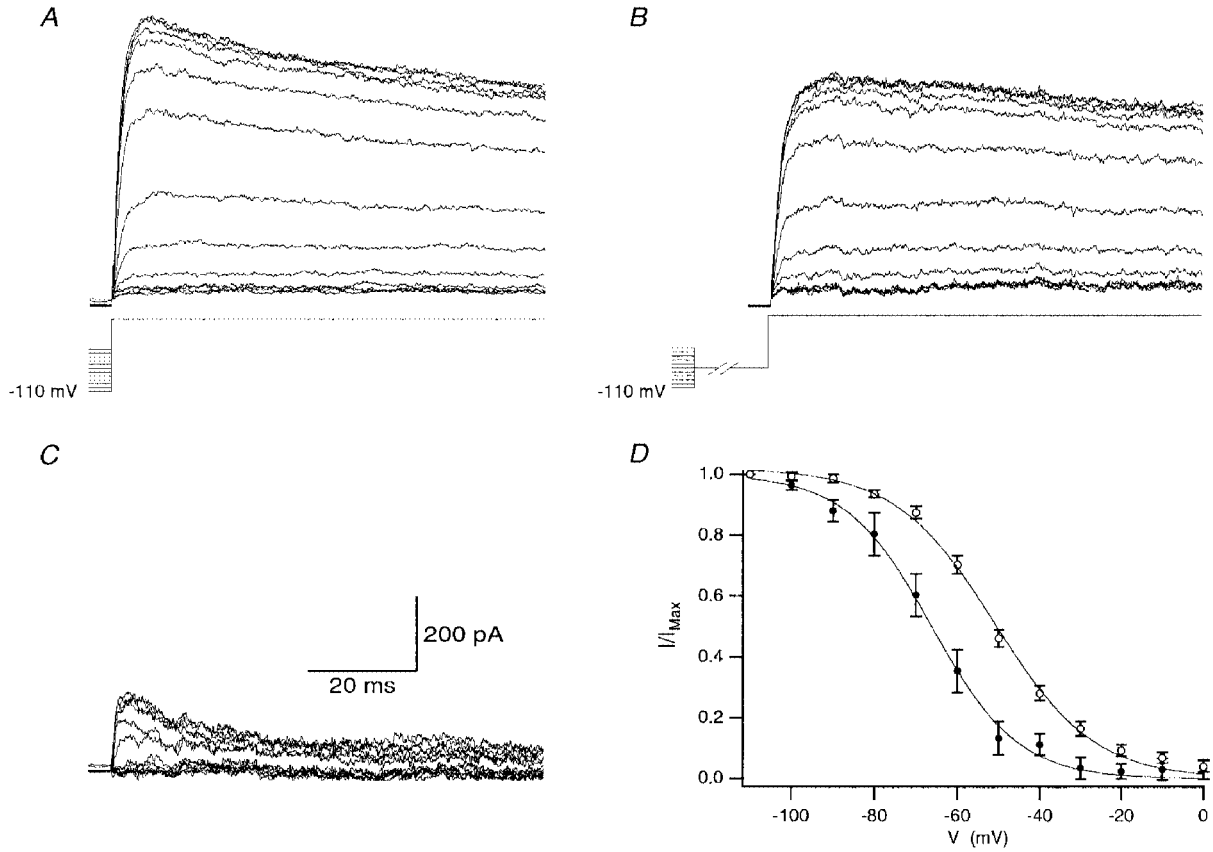

Figure 2. Inactivation of K^+ currents in nucleated patches

A, inactivation of outward currents recorded from a nucleated patch. Following a 15 s pre-pulse to voltages between −110 and 0 mV the patch was subjected to a 90 ms depolarising step to +80 mV (the voltage protocol is shown below the traces). Most of the pre-pulse was truncated to facilitate the display of the outward current. The voltage was stepped to −100 mV for 1 s after every sweep to allow K^+ channels to recover from inactivation (not shown). Records were sampled at 20 kHz and filtered at 5 kHz. Leak was subtracted off-line. *B*, currents obtained with a voltage protocol similar to that in *A* except for a 60 ms pulse to −50 mV inserted after the 15 s conditioning step to inactivate the fast K^+ current (the protocol is shown below the traces). Records were sampled at 20 kHz and filtered at 5 kHz. Leak was subtracted off-line. *C*, the difference current between the recordings shown in *A* and *B*. The scale bars also apply to *A* and *B*. *D*, inactivation curves of the slow K^+ current isolated in *B* (○) and the fast K^+ current isolated in *C* (●). The maximal current measured during every +80 mV voltage step was normalised to the maximal current measured at +80 mV following a step from −110 mV. The smooth lines are the fits to a Boltzmann function with one gate ($n = 5$). Error bars are ± S.E.M.

Table 2. Comparison between the kinetic and pharmacological separation of the fast K^+ current in nucleated patches

	Kinetic separation	Pharmacological separation
$V_{½}$ of activation (mV)	-3 ± 1 ($n = 5$)	0 ± 1 ($n = 11$)*
k of activation (mV)	20 ± 2 ($n = 5$)	$19 \pm 0{\cdot}7$ ($n = 11$)*
$V_{½}$ of inactivation (mV)	-66 ± 3 ($n = 5$)	-66 ± 2 ($n = 5$)*
k of inactivation (mV)	-10 ± 1 ($n = 5$)	-10 ± 1 ($n = 5$)*
τ of inactivation (ms)	$8{\cdot}2 \pm 0{\cdot}6$ ($n = 5$)	$8{\cdot}7 \pm 0{\cdot}5$ ($n = 6$)*

Numerical values are given as means ± S.E.M.* Measured in the presence of 30 mM TEA.

the fast K^+ current. The time constants, extracted from this analysis, ranged from $0{\cdot}31 \pm 0{\cdot}03$ ms at +80 mV ($n = 5$) to $1{\cdot}3 \pm 0{\cdot}2$ ms at −50 mV ($n = 5$) and displayed a bell-shaped dependence on voltage (Fig. 4*C*).

To measure the time constant of inactivation of the fast K^+ current the kinetic separation protocol (Fig. 1) was repeated in the presence of 10 mM TEA. Under these conditions, of reduced slow K^+ current amplitude, the fast current decayed mono-exponentially to the holding current (Fig. 5*A*). The inactivation time constant of the fast K^+ current was measured by mono-exponential fits to the decay phase of the current (Fig. 5*A*). Above −20 mV the inactivation time constant was not dependent on voltage with a mean value of $8{\cdot}0 \pm 0{\cdot}3$ ms ($n = 5$).

The rate of recovery from inactivation was measured by a modified dual voltage protocol (Fig. 5*B*) in the presence of 30 mM TEA. The residual slow K^+ current was estimated by a voltage step to +60 mV. The patch was then hyperpolarised for varying durations and the relative recovery from inactivation was measured by a second step to +60 mV (Fig. 5*B*). The rate of recovery from inactivation ranged from $12{\cdot}6 \pm 1{\cdot}5$ ms ($n = 5$) at −110 mV to 64 ± 11 ms ($n = 4$) at −70 mV. The rate of recovery from inactivation was well approximated by a mono-exponential fit to the maximal current amplitude obtained during the second step to +60 mV. The rate of inactivation between −70 mV and −40 mV was measured (in the presence of 30 mM TEA) by stepping the voltage for varying duration to the test potential, following a step to −110 mV, and then

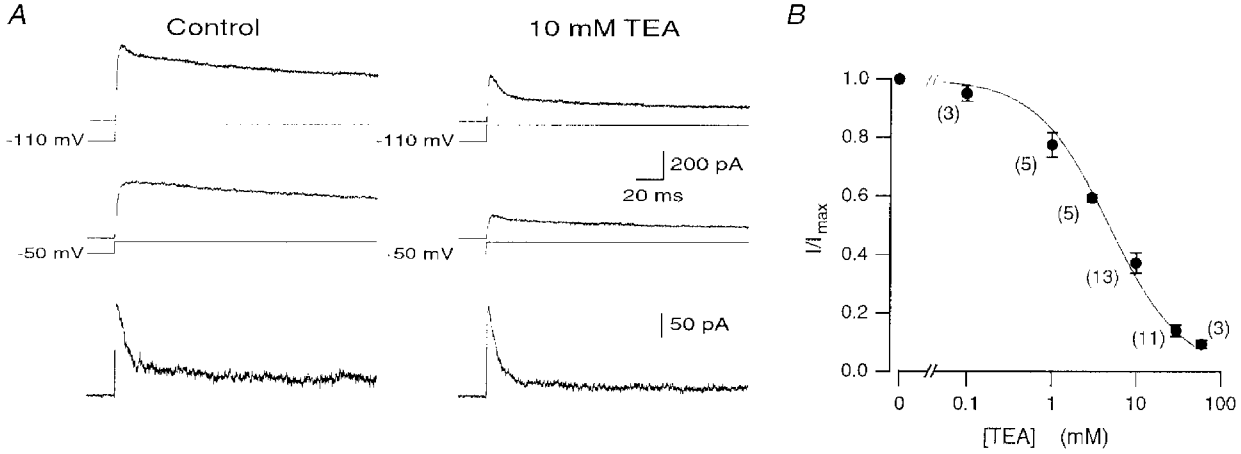

Figure 3. TEA blocks a slow K^+ current

A, the effect of 10 mM TEA on the two kinetically separated currents. Total outward current, measured at +80 mV following a pre-pulse to −110 mV (top traces) and with a 60 ms pulse to −50 mV inserted after that pre-pulse (middle traces). The fast K^+ current, given by the difference between the top two traces, is shown in the bottom traces. The control experiment is shown on the left side and the currents recorded from the same patch in the presence of 10 mM TEA are shown on the right. Filtered at 5 kHz and sampled at 20 kHz. Leak was subtracted off-line. The voltage steps are shown below the traces. *B*, concentration dependence curve of block by TEA. The line is a fit of the equation: $I/I_{max} = IC_{50}/(IC_{50} + [TEA])$. I is the current remaining after application of a given TEA concentration, I_{max} is the maximal current in the absence of TEA and IC_{50} (5 ± 1 mM) is the concentration of TEA yielding half the current observed under control conditions. The number of observations at each TEA concentration is indicated in parentheses next to the relevant data point. Error bars are ± S.E.M.

Table 3. Comparison between the kinetic and pharmacological separation of the slow K^+ current in nucleated patches

	Kinetic separation	Pharmacological separation
$V_{½}$ of activation (mV)	-3 ± 1 ($n = 5$)	-1 ± 2 ($n = 6$)*
k of activation (mV)	10 ± 1 ($n = 5$)	12 ± 1 ($n = 6$)*
$V_{½}$ of inactivation (mV)	-51 ± 4 ($n = 5$)	-54 ± 2 ($n = 5$)†
k of inactivation (mV)	-12 ± 2 ($n = 5$)	-11 ± 1 ($n = 5$)†

Numerical values are given as means ± S.E.M. * Measured in the presence of 10 mM 4-AP. † Measured in the presence of 3 mM 4-AP.

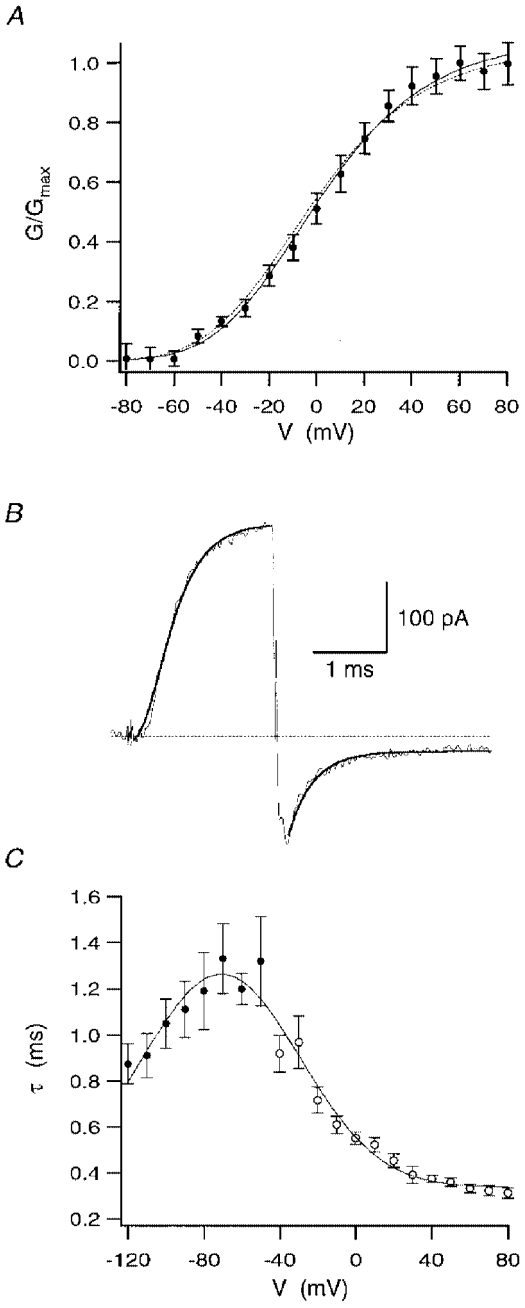

Figure 4. Activation kinetics of the fast K^+ current

A, activation curve of the fast current that was calculated from 5 experiments similar to the one shown in Fig. 1 in the presence of 30 mM TEA. G_{max} was $1 \pm 0{\cdot}2$ nS. Fit of the Boltzmann equation with four gates gave a $V_{½}$ of -47 ± 5 mV and $k = 29 \pm 4$ mV (smooth line). The curve fit of the activation curve of the fast current from Fig. 1 is shown as a dotted line for comparison. *B*, current recording of the activation and deactivation processes of the fast K^+ current. The fast outward current was generated by a 2 ms voltage step to +80 mV following a 50 ms pre-pulse to −110 mV. The voltage was then stepped to −120 mV to record the deactivation kinetics. The bath solution contained 30 mM TEA and 65 mM K^+. The increased K^+ concentration in the bath was used to generate larger tail currents. The smooth lines are the fits of a fourth order Hodgkin-Huxley model to the data. The time constants obtained from these fits were 0·33 ms and 1 ms for activation and deactivation, respectively. Since the tail current was fitted with a fourth order Hodgkin-Huxley model the time constant is 4 times slower than the time constant obtained by a mono-exponential fit. Series resistance compensation of 70 % was employed. The data are an average of 10 consecutive sweeps. Filtered at 10 kHz and sampled at 100 kHz. Leak was subtracted off-line. *C*, activation (○, $n = 10$) and deactivation (●, $n = 8$) time constants determined from traces similar to the one displayed in *B*. Errors bars are ± S.E.M. The smooth line is the curve fit to the equation: $C_1 + C_2\exp(-\{(V - C_3)/C_4\}^2)$, with $C_1 = 0{\cdot}34 \pm 0{\cdot}03$ ms, $C_2 = 0{\cdot}92 \pm 0{\cdot}04$ ms, $C_3 = -71 \pm 2$ mV and $C_4 = 59 \pm 4$ mV.

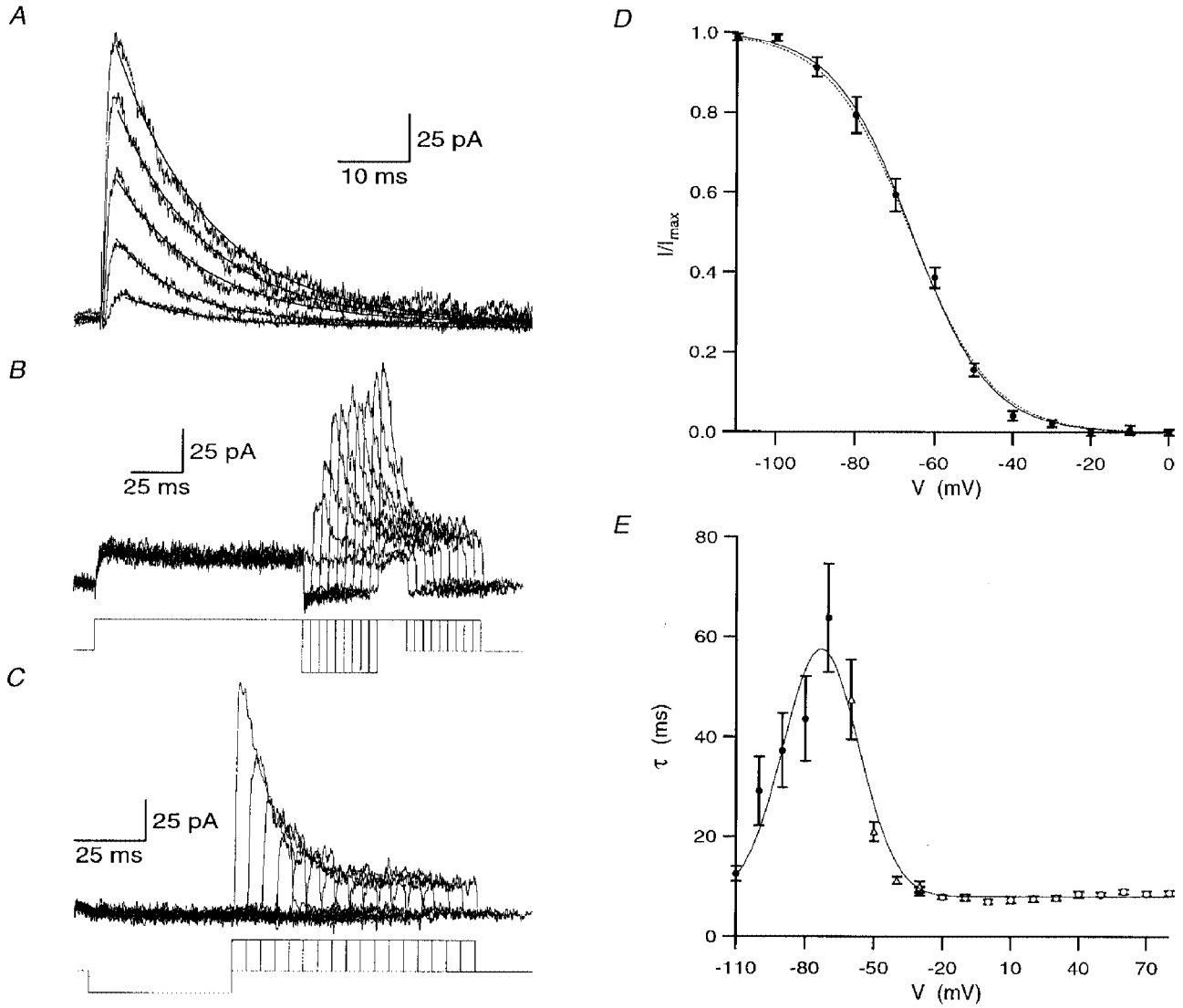

Figure 5. Inactivation kinetics of the fast K^+ current

A, current traces recorded following voltage steps from −110 mV to −20, 0, 20, 40 and 60 mV. The currents were recorded in the presence of 10 mM TEA. The residual slow K^+ current under these conditions was subtracted using a similar protocol to that shown in Fig. 1. The smooth lines are the curve fits to a mono-exponential decay. The time constants obtained from these fits were 7·5, 9, 12, 11 and 12 ms for −20, 0, 20, 40 and 60 mV, respectively. Filtered at 10 kHz and sampled at 50 kHz. Leak was subtracted off-line. *B*, recovery from inactivation. Following a 100 ms pulse to +60 mV (from a holding of −40 mV) the voltage was stepped for increasing intervals to −110 mV. This was followed by a 50 ms pulse to +60 mV. Leak was subtracted on-line using a *P*/4 protocol. The time constant calculated from the displayed data was 10 ms. The bath solution contained 30 mM TEA. The voltage clamp protocol is shown below the traces. Filtered at 5 kHz and sampled at 20 kHz. The voltage clamp protocol is shown below the traces. *C*, rate of inactivation at voltages where current was not detected. Following a 50 ms pre-pulse to −110 mV the voltage was stepped for varying durations to −40 mV and then for 20 ms to +60 mV. Leak was subtracted on-line using a *P*/4 protocol. The time constant calculated from the displayed data was 10 ms. The bath solution contained 30 mM TEA. The voltage clamp protocol is shown below the traces. Filtered at 5 kHz and sampled at 20 kHz. *D*, inactivation curve that was obtained from 11 patches using a similar protocol to the one described in Fig. 2. The peak current measured at 80 mV was normalised to the maximal current obtained from a given series of pulses. The smooth line was calculated using the Boltzmann function. The curve fit of the inactivation curve of the kinetically separated fast K^+ current (Fig. 2) is shown as a dotted line. *E*, inactivation time constant calculated from recovery from inactivation protocols (●, $n = 4$), pre-pulse inactivation protocols (△, $n = 5$), and from fitting a single exponential to the decay phase of the fast current (○, $n = 9$). The continuous line was calculated by a fit of the equation: $C_1 + C_2\exp(-\{(V - C_3)/C_4\}^2)$, with $C_1 = 8 \pm 1$ ms, $C_2 = 49 \pm 3$ ms, $C_3 = -73 \pm 1$ mV and $C_4 = 23 \pm 2$ mV.

to +60 mV to measure the current amplitude (Fig. 5*C*). As in Fig. 5*B* the rate of inactivation was calculated by mono-exponential fits to the maximal current amplitude at +60 mV. The inactivation time constant obtained from the previously mentioned voltage protocols displayed a bell-shaped dependence on voltage (Fig. 5*E*). The inactivation curve of the fast K^+ current was measured in the presence of 30 mM TEA using similar subtraction protocols as shown in Fig. 2. The values of $V_{½}$ and k obtained from a fit to a Boltzmann function with a single gate were -66 ± 2 mV and -10 ± 1 mV ($n = 5$), respectively. These values were not significantly different from the values obtained in the absence of TEA ($P = 1$ for $V_{½}$ and k, ANOVA, Fig. 2*D* and Table 2).

Block of a fast K^+ current by 4-AP

The effect of 4-AP was investigated using voltage protocols similar to those described above. 4-AP (3 mM) reduced the maximal amplitude of both fast and slow K^+ currents as recorded following a voltage step to +80 mV (Fig. 6*A*). The inactivation time constant of the fast K^+ current was 8 ± 2 ms ($n = 5$) and $9{\cdot}3 \pm 2$ ms ($n = 4$) at 1 and 3 mM 4-AP, respectively. These values were not significantly different from those obtained from the kinetic separation procedure ($P = 0{\cdot}92$ and 0·57 for 1 and 3 mM 4-AP, respectively, ANOVA). The inactivation time constant was not evaluated at higher 4-AP concentrations because of the small amplitude of the current. The concentration of 4-AP yielding half the current observed under control conditions was $4{\cdot}2 \pm 0{\cdot}5$ mM (Fig. 6*B*). The amplitude of the slow K^+ current was reduced by 30 mM 4-AP to $73 \pm 5\%$ ($n = 4$) of the control values (Fig. 6*B*). Since higher concentrations of 4-AP were not tested the data were not fitted to obtain the IC_{50}. 4-AP (10 mM) had no effect on the activation curve of the slow K^+ current (Fig. 7*A*). The $V_{½}$ of -1 ± 2 mV and k of 12 ± 1 mV ($n = 6$, Boltzmann function with one gate) were not significantly different from those determined using the kinetic separation protocol ($P = 0{\cdot}42$ for $V_{½}$ and 0·2 for k, ANOVA, Table 3). The activation kinetics of the slow K^+ current were quantified based on a Hodgkin-Huxley kinetic model in the presence of 9 mM 4-AP and 65 mM K^+ in the ACSF. A Hodgkin-Huxley model with two activation gates (Fig. 7*B*) best described the time course of activation and deactivation of the slow K^+ current. The time constants ranged from $2{\cdot}4 \pm 0{\cdot}3$ ms at +80 mV to 53 ± 4 ms at −50 mV and were fitted with a single exponential above −50 mV and another exponential below −50 mV (Fig. 7*C*).

The inactivation time constant of the slow K^+ current was measured by fitting the decay phase of the current to a double exponential function as shown in Fig. 7*A*. A pre-pulse of 60 ms to −50 mV was used to inactivate the fast K^+ current (Fig. 8*A*). Similar results were obtained when 9 mM 4-AP was used to block the fast K^+ current ($n = 5$). Current traces recorded following voltage pulses smaller than −10 mV were best fitted with a single exponential. The slow time constant, obtained from the double exponential curve fit, was slightly voltage sensitive and had a relative contribution of $57 \pm 5\%$ to the current ($n = 5$, Fig. 8*D*) that

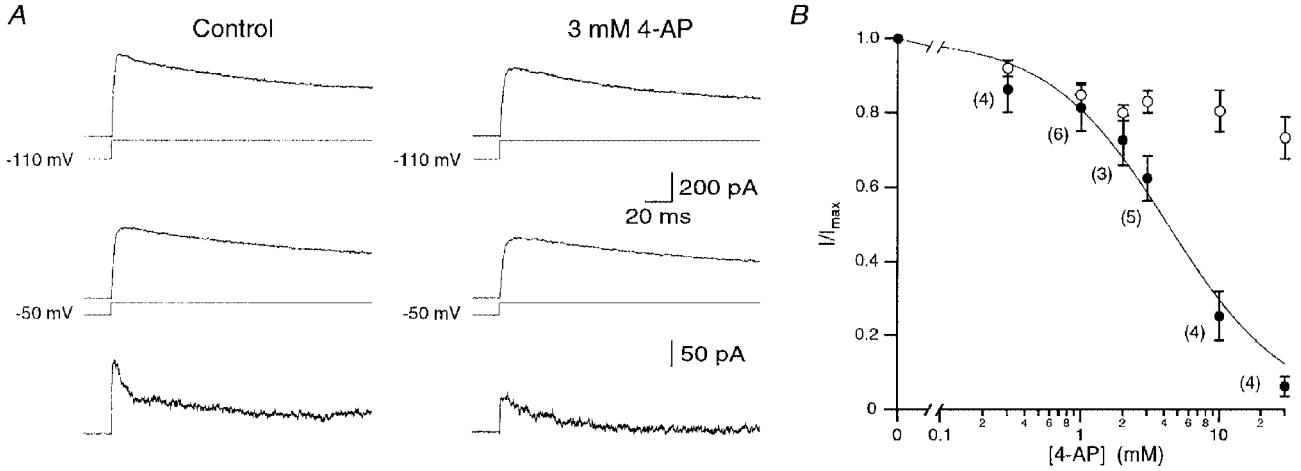

Figure 6. Block of the fast K^+ current by 4-AP

A, evaluation of the blocking effect of 3 mM 4-AP on the two K^+ currents. The total outward current, measured at +80 mV following pre-pulse to −110 mV (top traces) and with a 60 ms pulse to −50 mV inserted after that pre-pulse (middle traces). The fast K^+ current, given by the difference between the top two traces, is shown in the bottom traces. The control experiment is shown in the left traces and the currents recorded from the same patch in the presence of 3 mM 4-AP are shown in the right traces. Filtered at 5 kHz and sampled at 20 kHz. Leak was subtracted off-line. The voltage steps are shown below the traces. *B*, dose–response curve of the block of the fast K^+ current by 4-AP. The filled symbols are the normalised (to control) mean peak current, recorded after a voltage step to +80 mV, following bath application of 4-AP at a given concentration. The open symbols represent the normalised mean reduction in the slow K^+ current. The smooth line is a fit of the equation: $I/I_{max} = IC_{50}/(IC_{50} + [4\text{-AP}])$. The IC_{50} obtained from this fit was $4{\cdot}2 \pm 1$ mM. Error bars are S.E.M.

was independent of voltage. The faster time constant was more dependent on voltage ranging from 1100 ± 80 ms ($n = 6$) at −10 mV to 290 ± 50 ms ($n = 4$) at +80 mV. To estimate the time constant of recovery from inactivation a modified double voltage protocol was used (Fig. 8*B*) in the presence of 9 mM 4-AP to block the fast K^+ current. Most nucleated patches were unstable when frequently subjected to hyperpolarised voltages. To avoid patch deterioration, the first hyperpolarising pre-pulse in the double pulse protocol was omitted and the patch was held at −60 mV (Fig. 8*B*). The time constant of recovery from inactivation was calculated from mono-exponential fits of the maximal current amplitude during the second depolarising voltage step. The rate of recovery from inactivation ranged from 215 ± 12 ms ($n = 6$) at −110 mV to 1240 ± 230 ms ($n = 4$) at −70 mV. The inactivation curve of the slow K^+ current was measured in the presence of 3 mM 4-AP using similar subtraction protocols to those in Fig. 2. The $V_{½}$ and k obtained from a fit to a Boltzmann function with one gate were −54 ± 2 mV and −11 ± 1 mV ($n = 5$), respectively (Fig. 8*C* and Table 3). These values were not significantly different from the values obtained from the kinetic separation protocols ($P = 0{\cdot}52$ for $V_{½}$ and 0·67 for k, ANOVA, Table 3).

In addition to TEA and 4-AP, several selective K^+ channel toxins were tested. MCD-P (1 μM, $n = 4$), BDS-I (100 nM, $n = 3$), TsTx Kα (200 nM, $n = 3$), MgTx (300 nM, $n = 3$), StTx (300 nM, $n = 3$) and AgTx (60 nM, $n = 3$) had no effect on either the fast or the slow K^+ currents. DTX-I (250 nM, $n = 4$) reduced the amplitude of the slow K^+ current to 84 ± 7 % of the control values without affecting its activation or inactivation curves (data not shown). DTX-I did not affect the fast K^+ current.

K^+ channel types at the soma

The types and spatial distribution of the voltage-gated K^+ channels on the soma and apical dendrite were characterised in two phases by cell-attached measurements. First, the different channel types were investigated. To differentiate

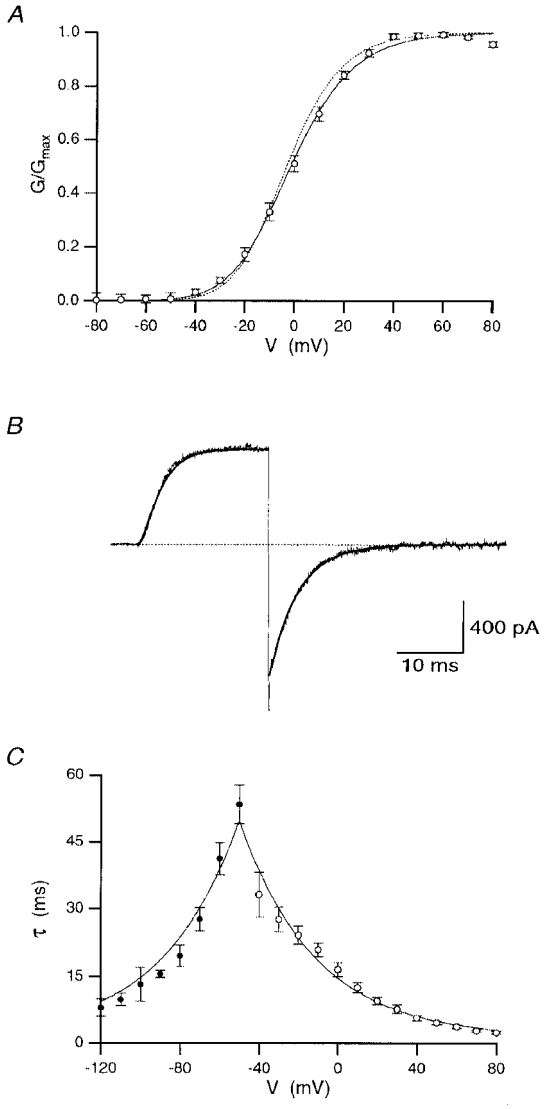

Figure 7. Activation kinetics of the slow K^+ current

A, the activation curve of the slow current that was calculated from 5 experiments in the presence of 3 mM 4-AP. G_{max} was 2·9 ± 0·3 nS. Fit of the Boltzmann function with two gates gave a $V_{½}$ of −14·3 ± 0·9 mV and a slope factor of $k = 14{\cdot}6 \pm 1{\cdot}0$ mV is shown as a continuous line. Error bars are S.E.M. The curve fit of the activation curve of the fast current from Fig. 1 is shown as a dotted line for comparison. *B*, activation and deactivation of the slow K^+ current. The outward current was generated by a 20 ms voltage step to +80 mV following a 400 ms pre-pulse to −110 mV. The voltage was then stepped to −120 mV to record the deactivation kinetics. The bath solution contained 10 mM 4-AP and 65 mM K^+. The smooth lines are the fits of a second order Hodgkin-Huxley model to the data. The time constants obtained from these fits were 2·5 and 8·5 ms for activation and deactivation, respectively. Series resistance compensation of 60 % was employed. Leak was subtracted off-line. Filtered at 10 kHz and sampled at 50 kHz. *C*, activation (○, $n = 11$) and deactivation (●, $n = 9$) time constants determined from traces similar to the one displayed in *B*. The deactivation time constants were fitted to: $C_1 + C_2 \exp(-C_3 V)$, with $C_1 = 1{\cdot}25 \pm 0{\cdot}1$ ms, $C_2 = 1{\cdot}15 \pm 0{\cdot}1$ ms and $C_3 = -0{\cdot}026 \pm 0{\cdot}01$ mV^{-1}. The activation time constants together with the deactivation time constant at −50 mV were fitted to the same equation to obtain $C_1 = 1{\cdot}25 \pm 0{\cdot}1$ ms, $C_2 = 13 \pm 1$ ms and $C_3 = 0{\cdot}026 \pm 0{\cdot}01$ mV^{-1}. Error bars are S.E.M.

between types, recordings were made with the aim of obtaining patches with only one type of channel and preferably only one apparent channel per patch. The channel types were sorted by their unitary conductance and inactivation kinetics. Out of 57 somatic cell-attached patches 10 displayed apparent single channel activity following a 120 mV depolarising voltage step (~+60 mV assuming a resting membrane potential of −60 mV) to fully activate voltage-gated K^+ channels.

In three patches channel openings were observed with short first latency (Fig. 9*A*). Following several openings the channels entered a long closed duration (Fig. 9*A*). The unitary conductance of this channel was 13 ± 1 pS (Fig. 9*C*, $n = 3$). Ensemble currents revealed a fast inactivating current (Fig. 9*B*). The decay of the current was fitted to a single exponent with time constants of 36 ms at 60 mV above the resting membrane potential, 28 ms at 80 mV and 34 ms at 100 mV (Fig. 9*B*). Similar time constants were

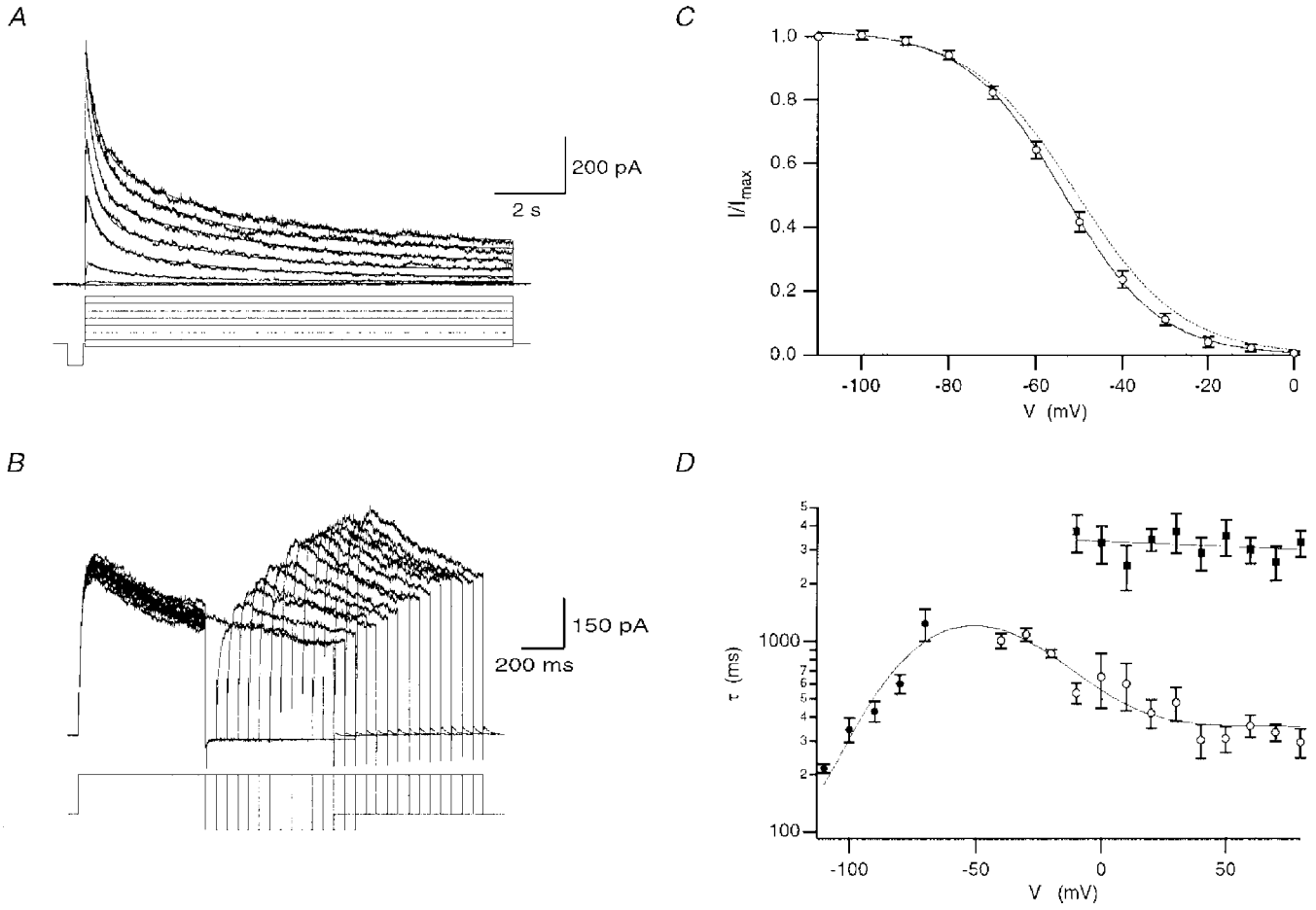

Figure 8. Inactivation kinetics of the slow K^+ current

A, 12 s long voltage steps from −60 to +60 mV with 20 mV intervals. A 500 ms pulse to −110 mV that was followed by a 60 ms pulse to −50 mV preceded the long steps. Data were sampled at 500 Hz and filtered at 100 Hz. The smooth lines are curve fits of a double exponential function. *B*, the rate of recovery from inactivation was measured, as for the fast current, by a double pulse protocol. The holding potential was −60 mV. The voltage was stepped for 600 ms to +40 mV. The voltage was then stepped to −100 mV for varying durations and back to +40 for 600 ms. Leak was not subtracted. The recording was carried out in the presence of 9 mM 4-AP. The time constant obtained from the experiment shown in Fig. 8*B* was 270 ms. *C*, inactivation curve of the slow K^+ current. The curve was determined using voltage protocols similar to those shown in Fig. 2 with 3 mM 4-AP in the bath ($n = 5$). The smooth line is the curve fit of the Boltzmann equation with $V_{½} = -54 \pm 2$ and $k = -11 \pm 1$. The dotted line is the curve fit of the Boltzmann function to the slow K^+ current from Fig. 2*D*. *D*, the time constant for recovery from inactivation (●, $n = 3$–6) and the two time constants obtained from the double exponential fit of the response to the long pulses (■ and ○, $n = 3$–6) displayed as a function of voltage. The slow component was fitted with a straight line with a slope of 4 ± 3 mV and an intercept of 3330 ± 400 mV. The faster component was fitted to the equation: $C_1 + (C_2 + C_5(V - C_6))\exp(-\{(V - C_3)/C_4\}^2)$, with $C_1 = 360 \pm 50$ ms, $C_2 = 1010 \pm 100$ ms, $C_3 = -75 \pm 5$ mV, $C_4 = 48 \pm 4$ mV, $C_5 = 24 \pm 2$ ms mV^{-1} and $C_6 = -55 \pm 3$ mV.

observed in two more patches that also contained other types of channels (see also Fig. 12). This inactivation time constant was four times larger than the time constant obtained in this voltage range for the fast K^+ current in nucleated patches (Figs 1 and 6).

In four patches a channel that displayed a long latency to the first opening when the voltage was stepped to 40 mV above the resting membrane potential (Fig. 10*A*) was observed. Burst duration increased while the intra-burst closed time decreased as a function of the applied voltage (Fig. 10*A*). The unitary conductance of this channel was 16 ± 1 pS (Fig. 10*B*, $n = 4$). A long closed duration was observed in most traces when voltage steps of 5 s to +60 mV above the resting membrane potential were applied (Fig. 10*C*). Summation of 45 sweeps revealed a slowly inactivating ensemble current (Fig. 10*C*). The decay of the ensemble current was best fitted to a single exponent with a time constant of $5{\cdot}5 \pm 2$ s at +60 mV above the resting membrane potential ($n = 3$). This time constant was similar to the slow time constant of the macroscopic current in nucleated patches zero mV ($3{\cdot}5 \pm 0{\cdot}8$ ms, $n = 6$, Fig. 8).

Channels that displayed a long latency to the first opening, when the voltage was stepped to 40 mV above the resting membrane potential (Fig. 11*A*), were observed in three additional patches. The unitary channel current at this voltage was smaller than that observed for the delayed channel described in Fig. 10. The unitary conductance of this channel was $9{\cdot}5 \pm 0{\cdot}5$ pS (Fig. 11*C*, $n = 3$). The rate of inactivation of these channels was faster than that found for the 16 pS channel (Fig. 10). The inactivation time constant, determined from ensemble currents, was 190 ms at 40 mV above the resting membrane potential, 130 ms at 60 mV,

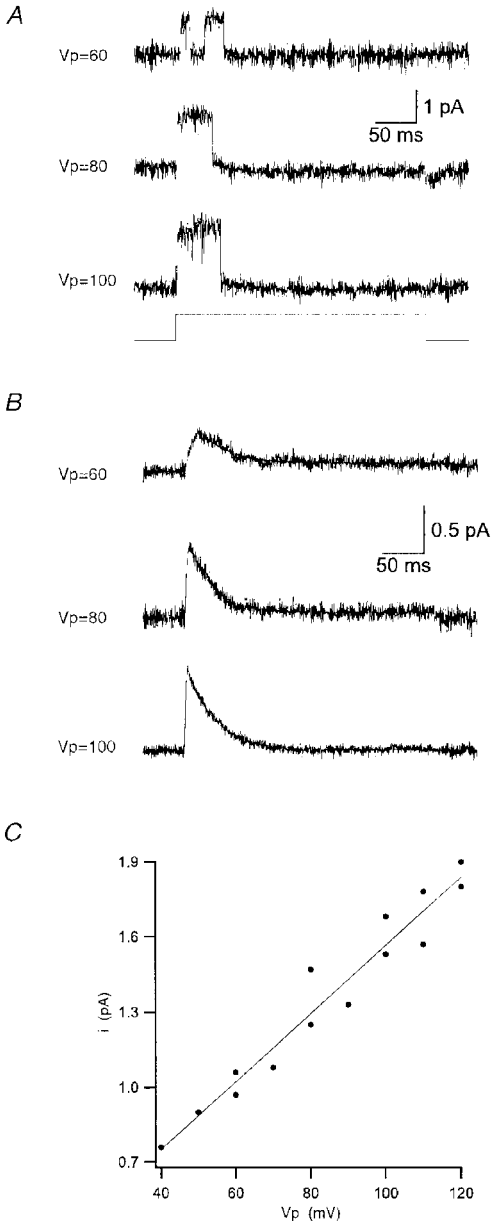

Figure 9. Cell-attached measurement of a fast inactivating channel at the soma

A, outward currents of a channel in a cell-attached patch following a 300 ms depolarising voltage step (V_p) to 60, 80 and 100 mV above the resting membrane potential. The holding potential was 20 mV below the resting membrane potential. The data were filtered at 2 kHz and sampled at 10 kHz. Leak and capacitance currents were reconstructed from empty traces. *B*, ensemble currents generated from the same experiment in which the traces shown in *A* were recorded. The ensemble currents are an average of 40 ($V_p = 60$ mV), 163 ($V_p = 80$ mV) and 191 ($V_p = 100$ mV) traces. The smooth lines are the curve fits of the data to a mono-exponential decay. *C*, current–voltage relationship obtained from 3 cell-attached patches of the type shown in *A*. The single channel current amplitudes displayed as a function of the voltage steps (V_p) indicated above to the resting membrane potential. The straight line is the linear regression line from which the single channel conductance was calculated as 13 ± 1 pS ($n = 3$).

and 200 ms at 80 mV (Fig. 11*B*). The inactivation time constant at 120 mV above the resting membrane potential was calculated to be 250 ± 50 ms ($n = 3$). These values were similar to the faster inactivation time constant of the slow K^+ current in nucleated patches (Fig. 8).

K^+ channel distribution along the apical dendrite

The types and density of K^+ channels along the apical dendrite were also investigated with cell-attached recordings. The patches were subjected to voltage steps to 140 mV above the resting membrane potential. Assuming a resting membrane potential of −60 mV the voltage across the patch was about +80 mV. At this voltage the channel open probability should have been maximal and insensitive to changes in the resting membrane potential during the experiments and between cells. Moreover, at this voltage, activation of voltage-gated Ca^{2+} channels should result in little Ca^{2+} influx. Therefore, the concentration of intracellular Ca^{2+} was not expected to increase considerably and the opening probability of Ca^{2+}-gated K^+ channels was expected to remain low.

Considerable variability was observed between patches along the apical dendrite. Out of the 61 patches along the dendrite 10 did not have any outward current and 14 displayed currents that appeared to result from the activation of a single channel. In another 28 patches it was possible to observe, in some sweeps, unitary channel openings even when the patch contained more than one channel. The variability in current size and time course of currents recorded in different patches from the same neurone probably reflected a low channel density. Since pipettes of similar open tip resistance were used for somatic and dendritic patches a difference in the patch area was not very likely. Channel openings that could be clearly differentiated were associated by their unitary current magnitude to one of the three types observed at the soma. Eight such recordings are shown in Fig. 12. These recordings are from patches that displayed low channel activity. They represent, therefore, the types of channels observed along the apical dendrite rather than the current density. In three patches brief channel openings that were followed by a long closed duration were observed (at 25, 55 and 125 μm away from

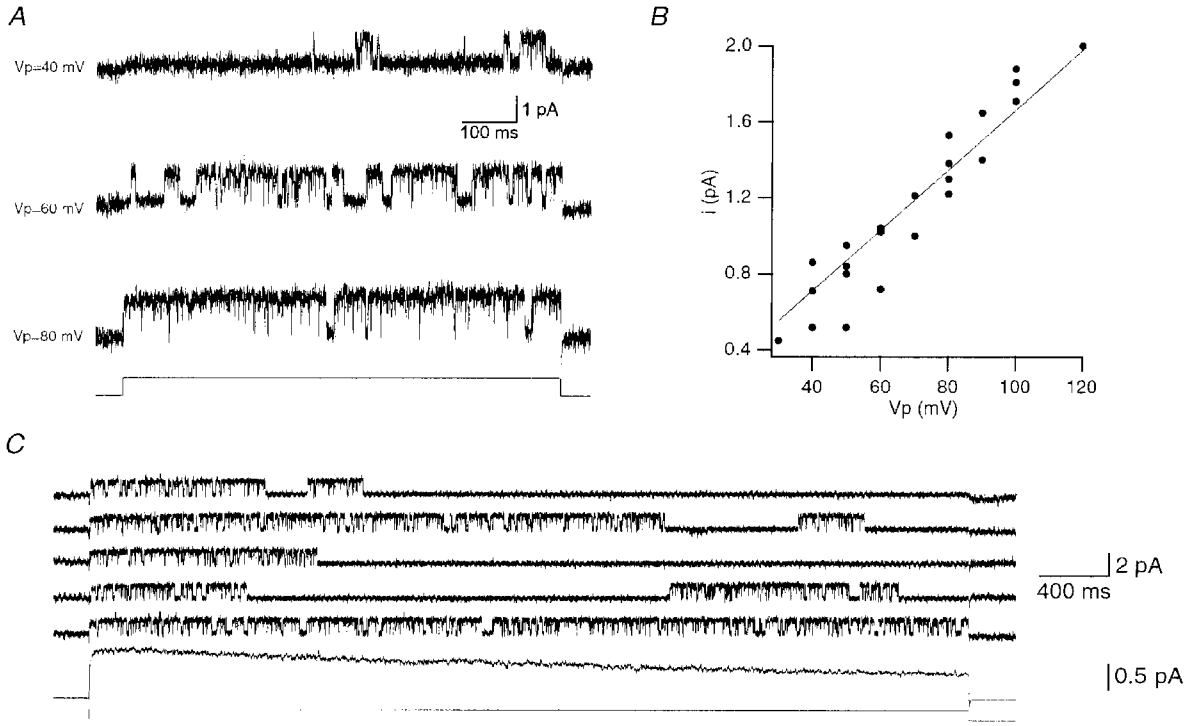

Figure 10. Cell-attached measurement of very slow inactivating outward currents at the soma

A, outward currents of a channel in a cell-attached patch following a 800 ms depolarising voltage step (V_p) to 40, 60 and 80 mV above the resting membrane potential. The holding potential was 20 mV below the resting membrane potential. Data were filtered at 2 kHz and sampled at 10 kHz. Leak and capacitance currents were reconstructed from empty traces. *B*, current–voltage relationship obtained from 4 cell-attached patches of the type shown in *A*. The single channel current amplitudes displayed as a function of the voltage steps (V_p) indicated above to the resting membrane potential. The straight line is the linear regression line from which the single channel conductance was calculated as 16 ± 1 pS ($n = 4$). *C*, pulses of 5 s to 60 mV above the resting membrane potential. The data were filtered at 1 kHz and sampled at 10 kHz. Leak and capacitance currents were reconstructed from empty traces. The average of 45 traces is shown below the single channel traces. The average was filtered at 500 Hz to facilitate the display of the slow inactivation.

the soma). In two other patches a channel that was open for most of the depolarising pulse was observed (at 80 and 200 μm). This channel corresponded in unitary amplitude to the very slow K^+ channel reported in Fig. 10. In one patch (at 200 μm) a channel that was open for most of the duration of the depolarisation but had unitary amplitude similar to that of the slow K^+ channel reported in Fig. 11 was observed. In two patches (at 125 and 360 μm) several types of channel openings were observed in the recording. The three types of channels that were observed in the somatic recordings were also observed in the region that was investigated along the apical dendrite. The occurrence of these types of channels along the dendrite is summarised in Fig. 13*B*. Ensemble patch currents, measured by averaging 70–180 consecutive responses to step changes of 140 mV for each patch, are shown next to the single channel recording. These recordings confirm the association of the observed channels with one of the three channel types that were identified at the soma. The ensemble currents of the fast channel displayed a mono-exponential decay. The inactivation time constant of this fast channel varied from 16 to 48 ms at various recordings along the dendrite (mean 29 ± 3 ms, $n = 7$). The mean peak current in somatic patches, regardless of the types of channels that were observed in the patch, following a 140 mV voltage step was 5·5 ± 0·7 pA ($n = 40$). Assuming that at that voltage the channel opening probability approached unity and that the resting membrane potential was −60 mV, the peak conductance was 30 ± 4 pS.

In a previous study of dissociated neocortical pyramidal neurones (Kang *et al.* 1996) a patch area of 5–20 μm^2 was

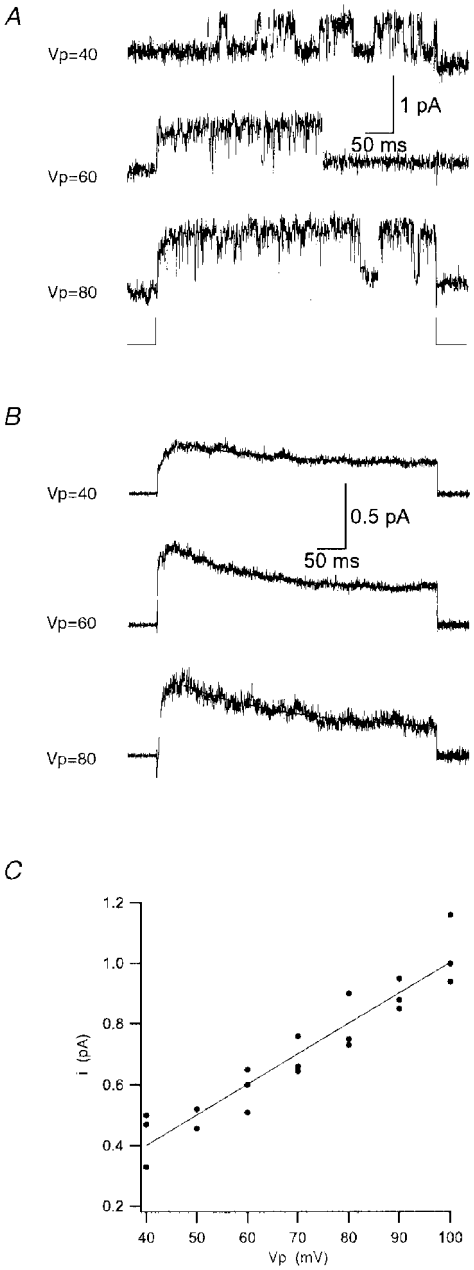

Figure 11. Cell-attached measurement of slow inactivating outward currents at the soma

A, outward currents of a channel in a cell-attached patch following a 400 ms depolarising voltage step (V_p) to 40, 60 and 80 mV above the resting membrane potential. The holding potential was 20 mV below the resting membrane potential. The data were filtered at 1 kHz and sampled at 10 kHz. Leak and capacitance currents were reconstructed from empty traces. *B*, ensemble currents generated from the same experiment in which the traces shown in *A* were recorded. The ensemble currents are an average of 107 ($V_p = 40$ mV), 150 ($V_p = 60$ mV) and 55 ($V_p = 80$ mV) traces. The smooth lines are the curve fits of the data to a mono-exponential decay. *C*, current–voltage relationship obtained from 3 somatic cell-attached patches of the type shown in *A*. The single channel current amplitudes displayed as a function of the voltage steps (V_p) indicated above to the resting membrane potential. The straight line is the linear regression line from which the single channel conductance was calculated as 9·5 ± 0·5 pS ($n = 3$).

reported albeit with slightly larger pipettes than those used in the present work. Using this patch area the total K^+ conductance density was calculated to be in the range 4–17 pS μm^{-2}, corresponding with the $6{\cdot}6 \pm 0{\cdot}7$ pS μm^{-2} estimated for nucleated patches (Fig. 1). The peak amplitude of the ensemble K^+ current changed as a function of the distance from the soma (Fig. 13*A*) with a slope of $-0{\cdot}9 \pm 0{\cdot}3$ pA $(100\ \mu m)^{-1}$ with a statistically significant ($P < 0{\cdot}01$) Spearman rank order correlation coefficient of $-0{\cdot}3$. The distribution of these channels as a function of the distance from the soma is shown in Fig. 13*A*.

In four patches (two somatic and two dendritic at 60 and 300 μm) a fourth type of K^+ channel was observed. This K^+ channel had a unitary conductance of approximately 150 pS ($n = 2$) matching that of the large conductance Ca^{2+}-activated K^+ (BK) channels observed in dissociated neocortical pyramidal neurones (Kang *et al.* 1996). The low frequency of occurrence of this K^+ channel subtype may be due to a lower channel density than the one reported for dissociated neocortical pyramidal neurones (Kang *et al.* 1996) or to a low channel opening probability due to a low intracellular Ca^{2+} concentration.

DISCUSSION

We investigated voltage-gated K^+ currents in the soma and apical dendrite of young L5 pyramidal neurones. Two classes of K^+ currents were separated in nucleated patches, a slow inactivating, TEA-sensitive current and a fast inactivating, 4-AP-sensitive current. Cell-attached recordings from the soma indicated that at least three channel types with different unitary conductances and inactivation kinetics mediated the fast and slow K^+ currents in nucleated soma

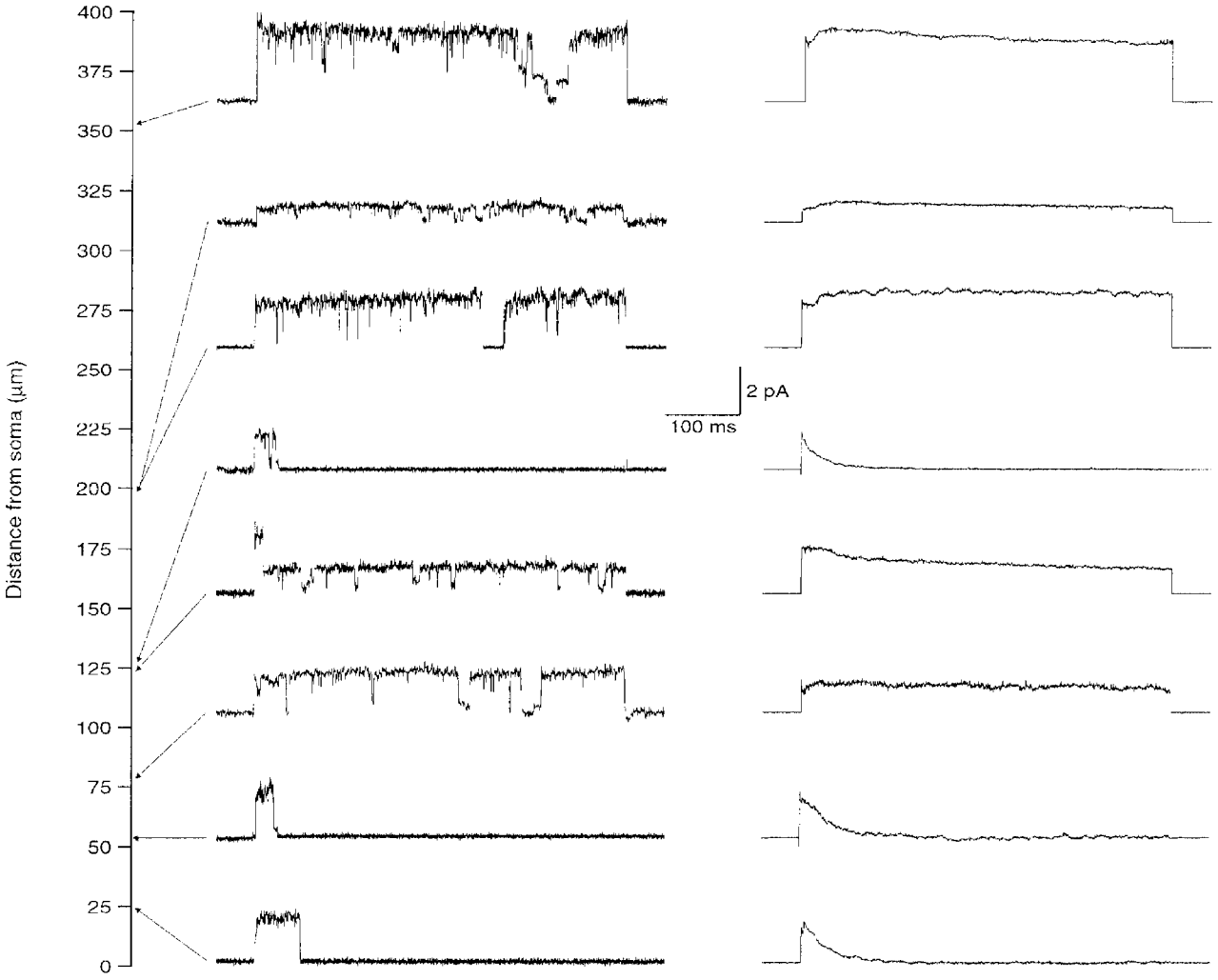

Figure 12. Cell-attached recording of K^+ currents along the apical dendrite

Eight recordings from dendritic cell-attached patches from 8 different neurones. The currents were evoked by a 500 ms depolarising voltage step to 140 mV above the resting membrane potential. The distance from the soma along the apical dendrite is shown on the left of the traces and an arrow indicates the distance of each trace. The traces were filtered at 1 kHz and sampled at 10 kHz. Leak and capacitative currents were subtracted off-line from empty traces. The ensemble currents obtained by averaging 70–180 consecutive responses are shown next to the single channel recording.

patches. The density of the outward K^+ current, estimated from cell-attached patch recordings up to a distance of 430 μm from the soma, decreased along the apical dendrite

K^+ current components

The voltage protocols used for the kinetic separation of the currents in Figs 1 and 2 are standard protocols. These protocols may produce incomplete separation and should be interpreted with caution. This was demonstrated by the difference between the kinetically separated fast K^+ current to that measured in the presence of TEA. When separated kinetically, the fast K^+ current decayed to a sustained current level (Figs 1 and 2). When the slow K^+ current was blocked by 10 mM TEA the fast K^+ current decayed back to the holding current (Fig. 5*A*).

The time constant of inactivation of the fast K^+ current was 21 ± 2 ms at -50 mV (Fig. 5). Following the 60 ms voltage pre-pulse to -50 mV the fast K^+ current should be 85% inactivated (Figs 2 and 5). The inactivation time constant of the slow K^+ current was approximately 1000 ms at -50 mV (Fig. 8). Following the 60 ms pre-pulse to -50 mV the slow K^+ current should be 5% inactivated (Figs 2 and 8). The mean peak conductance of the slow K^+ current was $2{\cdot}9 \pm 0{\cdot}3$ nS ($n = 5$). Thus, the total current inactivated following the 60 ms pre-pulse to -50 mV should have been ~30 pA (at + 80 mV). This corresponds to the amplitude of the sustained level of current observed for the fast K^+ current (Fig. 1).

This suggested that the sustained current observed following kinetic separation was not due to the activation of the fast K^+ current but rather the result of a small degree of inactivation of the slow K^+ current. In support of this conclusion, average currents obtained from single channel currents of the fast K^+ channel in cell-attached patches also displayed a mono-exponential inactivation back to the holding current (Fig. 9).

Kinetic separation of the two conductances that compose the slow K^+ current in nucleated patches would also not be entirely reliable. Initially the fast current would have to be inactivated leading to a 5% inaccuracy in the amplitude of the slow K^+ current. Then, to achieve complete inactivation of the slow K^+ channel voltage pulses longer than 1 s should be applied (Figs 8 and 11). However, the inactivation time constant of the very slow K^+ channel was 3–5 s (Figs 8 and 10). Therefore, any voltage pulse designed to inactivate the slow K^+ channel would also cause substantial inactivation of the very slow K^+ channel. It was previously reported, for dissociated neocortical pyramidal neurones and in nucleated patches from L5 pyramidal neurones (Hamill *et al.* 1991; Bekkers & Stuart, 1998), that the K^+ current was composed of two components, a fast inactivating K^+ current and a slow inactivating K^+ current (Hamill *et al.* 1991). The slow inactivating K^+ current displayed incomplete steady-state inactivation (Hamill *et al.* 1991). This observation differs from the complete steady-state inactivation reported here. It is possible that this difference is the result of the

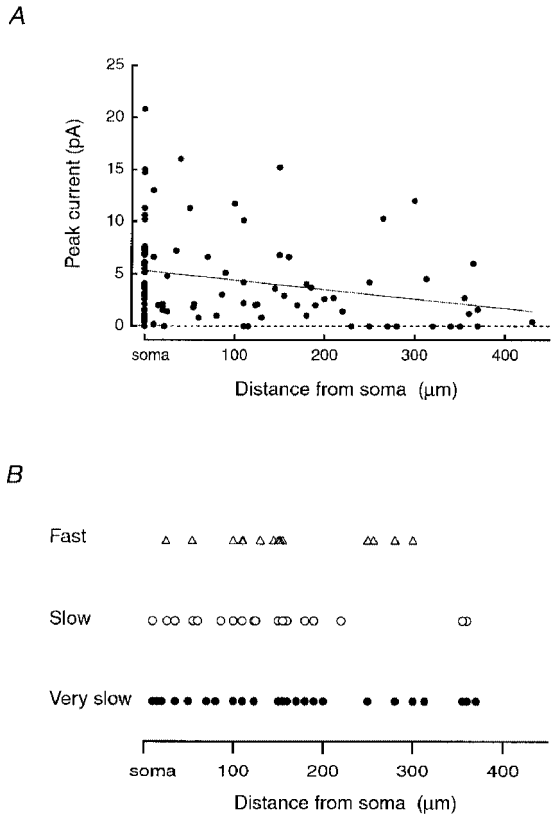

Figure 13. Distribution of the K^+ channels along the apical dendrite

A, peak amplitude of the average current as a function of the distance from the soma (●). Voltage steps to +140 mV above the resting membrane potential generated the currents. The smooth line is a linear regression that passed through the data points (somatic and dendritic). The slope was $-0{\cdot}9 \pm 0{\cdot}3$ pA (100 μm)$^{-1}$ with a regression coefficient of $-0{\cdot}3$. *B*, the distribution of the fast (△), slow (○) and very slow (●) inactivating K^+ conductances as a function of the distance from the soma. The conductances were classified as one of the three types reported in Figs 9–11 based on the difference in their unitary current following a voltage step to 140 mV above the resting membrane potential.

conditioning voltage steps used to measure the inactivation curve being shorter than those used here.

Molecular identity of K^+ channels

Previous studies revealed the expression of the voltage-gated K^+ channel subunits Kvα1.2, Kvα1.4 Kvα2.1, Kvβ1.1 and Kvβ2.1 in L5 neocortical pyramidal neurones (Sheng *et al.* 1994; Rhodes *et al.* 1995, 1996). The Kvα4.2 and Kvα4.3 subunits were detected in L5 of the neocortex although their exact cellular localisation remains to be determined (Tsaur *et al.* 1997; Serodio & Rudy, 1998). This diversity of channel subunits leads to the conclusion that native K^+ channels are heteromers, containing probably both α- and β-subunits. The subunit composition greatly affects the properties of K^+ channels (Ruppersberg *et al.* 1990; Rettig *et al.* 1994). Therefore it is not possible, at present, to derive the subunit composition of native K^+ channels by comparison of their functional properties with those of cloned and heterologously expressed K^+ channels. It will, however, be interesting to determine whether the decrease in the K^+ current amplitude along the apical dendrite (Fig. 13) is due to a decrease in the density of the heteromeric channels or to a decrease in the density of a particular subunit that is crucial for the channel assembly.

K^+ current kinetics

We attempted to provide a quantitative description of the currents in nucleated patches using the Hodgkin-Huxley formalism (Figs 4, 5, 7 and 8). This description is obviously incomplete. The slow K^+ current was satisfactorily described by a second order Hodgkin-Huxley model (Fig. 7). The observation that two types of K^+ conductances mediated the slow K^+ current will require further investigation of their individual kinetics. The widely used kinetic models of voltage-gated K^+ channels in simulations of neocortical pyramidal neurones (Mainen *et al.* 1995) differ considerably from the data reported here. The description provided here may, however, be a first step to obtain a better model of voltage-gated channels in neocortical pyramidal neurones. Recent observations from cell-attached recordings suggest that the three K^+ conductances reported here were activated by an action potential at the soma (Bekkers & Stuart, 1998; Kang *et al.* 2000). Thus dissection of the role of each conductance in the repolarisation of the action potential would greatly benefit from a kinetic model.

The data shown here suggest that further kinetic investigation of K^+ channels in neocortical pyramidal neurones should be pursued at the single channel level. The inactivation time constant of the slow and very slow inactivating K^+ channels measured from nucleated patches (Fig. 8) correspond to those obtained from cell-attached patches (Figs 10 and 11). However, both of these channels display many rapid closures within opening bursts (Figs 10 and 11). This may indicate that these channels have more than one closed state. Since kinetic separation of the slow K^+ current from the very slow K^+ current in nucleated patches is unreliable, and since no specific blocker was found for one of these currents, analysis of single channel data may be the best source for kinetic information on the two slow K^+ currents.

While the inactivation time constants of slower channels were comparable to those measured in nucleated patches the time constant of inactivation of the fast K^+ channel was almost 4-fold slower in cell-attached patches (Fig. 9) than in nucleated patches (Figs 1, 3 and 5). Moreover, this time constant varied in different recordings from the apical dendrite. The inactivation time constant in nucleated patches was similar after kinetic separation (Fig. 1) and after block of the slow K^+ current by TEA (Figs 3 and 5). Therefore, the difference in the inactivation time constant of the fast K^+ current between nucleated and cell-attached patches might be due to wash-out of cytoplasmic components in nucleated patch recordings. These observations also suggest that the fast K^+ current may be a target for modulation by intracellular second messengers or may be sensitive to the redox potential of the cell as was shown for other K^+ channels (Ruppersberg *et al.* 1991).

Distribution of K^+ channels

In pyramidal neurones of the CA1 region of the hippocampus the amplitude of a fast inactivating K^+ current has been shown to increase along the apical dendrite (Hoffman *et al.* 1997) and to control the amplitude of the back-propagating action potential and as a result the distance to which this action potential propagates into the apical dendrite. We report here that the three types of K^+ channels observed in cell-attached patches at the soma (Figs 9–11) were also observed along the apical dendrite up to a distance of 430 μm from the soma (Figs 12 and 13). The peak amplitude of the average ensemble currents from cell-attached patches decreased from the soma towards the distal portions of the apical dendritic trunk (Fig. 13). Based on the data shown in Figs 12 and 13, we would suggest that this decrease was the result of a decrease in the density of all three types of voltage-gated K^+ currents and not just that of one type. Furthermore, it was reported for dissociated neocortical pyramidal neurones that the density of the large conductance Ca^{2+}-activated K^+ channels was lower in the stump of the apical dendrite than at the soma (Kang *et al.* 1996). Collectively this may indicate that in neocortical pyramidal neurones the density of all K^+ channels decreases along the apical dendrite.

Functional significance

What may be the physiological consequences of a lower K^+ channel density in the distal apical tuft? In a recent study it has been demonstrated that coincidence of a distal synaptic input and a back-propagating action potential generated a dendritic Ca^{2+} spike in the distal portion of the apical dendrite of mature L5 pyramidal neurones (Larkum *et al.* 1999), which generated a burst of axonally initiated action potentials. This was consistent with the suggestion that the distal apical dendrite contained a higher density of voltage-gated Ca^{2+} channels (Amitai *et al.* 1993; Schiller *et al.* 1997;

Larkum *et al.* 1999). Previously it has been observed that the Na^+ channel density did not change significantly up to 530 μm away from the soma (Stuart & Sakmann, 1994). Given that the K^+ channel density decreases along the apical dendrite (Fig. 13), and assuming that adult neurones also display a gradient, an increase in the Ca^{2+} channel density alone may not be a necessary pre-condition for the generation of regenerative dendritic potentials. Thus the gradual decrease in the K^+ channel density may define a distal region along the apical dendrite with a lower threshold for the generation of regenerative potentials. This does not preclude the possibility that the density of voltage-gated Ca^{2+} channels is higher in the distal apical dendrite than at the soma. It is possible that the decrease in the density of K^+ channels reported here and the proposed increase in the density of voltage-gated Ca^{2+} channels combine to control the initiation and prolongation of regenerative potentials in the apical tuft of L5 pyramidal neurones.

Amitai, Y., Friedman, A., Connors, B. W. & Gutnick, M. J. (1993). Regenerative activity in apical dendrites of pyramidal cells in neocortex. *Cerebral Cortex* **3**, 26–38.

Bekkers, J. M. & Stuart, G. (1998). Distribution and properties of potassium channels in the soma and apical dendrites of layer 5 cortical pyramidal neurons. *Society for Neuroscience Abstracts* **24**, 2019.

Hamill, O. P., Huguenard, J. R. & Prince, D. A. (1991). Patch-clamp studies of voltage-gated currents in identified neurons of the rat cerebral cortex. *Cerebral Cortex* **1**, 48–61.

Hodgkin, A. L. & Huxley, A. F. (1952). A quantitative description of membrane current and its application to conduction and excitation in nerve. *Journal of Physiology* **117**, 500–544.

Hoffman, D. A., Magee, J. C., Colbert, C. M. & Johnston, D. (1997). K^+ channel regulation of signal propagation in dendrites of hippocampal pyramidal neurons. *Nature* **387**, 869–875.

Jan, L. Y. & Jan, Y. N. (1997). Cloned potassium channels from eukaryotes and prokaryotes. *Annual Review of Neuroscience* **20**, 91–123.

Kang, J., Huguenard, J. R. & Prince, D. A. (1996). Development of BK channels in neocortical pyramidal neurons. *Journal of Neurophysiology* **76**, 188–198.

Kang, J., Huguenard, J. R. & Prince, D. A. (2000). Voltage-gated potassium channels activated during action potentials in layer V neocortical pyramidal neurons. *Journal of Neurophysiology* **83**, 70–80.

Koester, H. J. & Sakmann, B. (1998). Calcium dynamics in single spines during coincident pre- and postsynaptic activity depend on relative timing of back-propagating action potentials and subthreshold excitatory postsynaptic potentials. *Proceedings of the National Academy of Sciences of the USA* **95**, 9596–9601.

Korngreen, A., Bergling, S. & Sakmann, B. (1999). Voltage gated potassium channels and back propagation of the action potential in layer V pyramidal neurons. *Biophysical Journal* **76**, A327.

Larkum, M. E., Zhu, J. J. & Sakmann, B. (1999). A novel cellular mechanism for coupling inputs arriving at different cortical layers. *Nature* **398**, 338–341.

Llinás, R. R. (1988). The intrinsic electrophysiological properties of mammalian neurons: insights into central nervous system function. *Science* **242**, 1654–1664.

Magee, J. C., Christofi, G., Miyakawa, H., Christie, B., Lasser-Ross, N. & Johnston, D. (1995). Subthreshold synaptic activation of voltage-gated Ca^{2+} channels mediates a localized Ca^{2+} influx into the dendrites of hippocampal pyramidal neurons. *Journal of Neurophysiology* **74**, 1335–1342.

Magee, J. C. & Johnston, D. (1995). Synaptic activation of voltage-gated channels in the dendrites of hippocampal pyramidal neurons. *Science* **268**, 301–304.

Mainen, Z. F., Joerges, J., Huguenard, J. R. & Sejnowski, T. J. (1995). A model of spike initiation in neocortical pyramidal neurons. *Neuron* **15**, 1427–1439.

Markram, H., Helm, P. J. & Sakmann, B. (1995). Dendritic calcium transients evoked by single back-propagating action potentials in rat neocortical pyramidal neurons. *Journal of Physiology* **485**, 1–20.

Markram, H. & Sakmann, B. (1994). Calcium transients in dendrites of neocortical neurons evoked by single subthreshold excitatory postsynaptic potentials via low-voltage-activated calcium channels. *Proceedings of the National Academy of Sciences of the USA* **91**, 5207–5211.

Neher, E. (1992). Correction for liquid junction potentials in patch clamp experiments. *Methods in Enzymology* **207**, 123–131.

Nicoll, R. A. (1988). The coupling of neurotransmitter receptors to ion channels in the brain. *Science* **241**, 545–551.

Rettig, J., Heinemann, S. H., Wunder, F., Lorra, C., Parcej, D. N., Dolly, J. O. & Pongs, O. (1994). Inactivation properties of voltage-gated K^+ channels altered by presence of β-subunit. *Nature* **369**, 289–294.

Rhodes, K. J., Keilbaugh, S. A., Barrezueta, N. X., Lopez, K. L. & Trimmer, J. S. (1995). Association and colocalization of K^+ channel α- and β-subunit polypeptides in rat brain. *Journal of Neuroscience* **15**, 5360–5371.

Rhodes, K. J., Monaghan, M. M., Barrezueta, N. X., Nawoschik, S., Bekele-Arcuri, Z., Matos, M. F., Nakahira, K., Schechter, L. E. & Trimmer, J. S. (1996). Voltage-gated K^+ channel β subunits: expression and distribution of Kvβ1 and Kvβ2 in adult rat brain. *Journal of Neuroscience* **16**, 4846–4860.

Ruppersberg, J. P., Schröter, K. H., Sakmann, B., Stocker, M., Sewing, S. & Pongs, O. (1990). Heteromultimeric channels formed by rat brain potassium-channel proteins. *Nature* **345**, 535–537.

Ruppersberg, J. P., Stocker, M., Pongs, O., Heinemann, S. H., Frank, R. & Koenen, M. (1991). Regulation of fast inactivation of cloned mammalian I_K(A) channels by protein phosphorylation. *Nature* **352**, 711–714.

Sakmann, B. & Neher, E. (1995). Geometric parameters of pipettes and membrane patches. In *Single Channel Recording*, ed. Sakmann, B. & Neher, E., pp. 637–650. Plenum Press, New York.

Sather, W., Dieudonne, S., MacDonald, J. F. & Ascher, P. (1992). Activation and desensitization of *N*-methyl-D-aspartate receptors in nucleated outside-out patches from mouse neurones. *Journal of Physiology* **450**, 643–672.

Schiller, J., Helmchen, F. & Sakmann, B. (1995). Spatial profile of dendritic calcium transients evoked by action potentials in rat neocortical pyramidal neurones. *Journal of Physiology* **487**, 583–600.

Schiller, J., Schiller, Y., Stuart, G. & Sakmann, B. (1997). Calcium action potentials restricted to distal apical dendrites of rat neocortical pyramidal neurons. *Journal of Physiology* **505**, 605–616.

Serodio, P. & Rudy, B. (1998). Differential expression of Kv4 K^+ channel subunits mediating subthreshold transient K^+ (A-type) currents in rat brain. *Journal of Neurophysiology* **79**, 1081–1091.

Sheng, M., Tsaur, M. L., Jan, Y. N. & Jan, L. Y. (1994). Contrasting subcellular localization of the Kv1.2 K^+ channel subunit in different neurons of rat brain. *Journal of Neuroscience* **14**, 2408–2417.

Spruston, N., Schiller, Y., Stuart, G. & Sakmann, B. (1995). Activity-dependent action potential invasion and calcium influx into hippocampal CA1 dendrites. *Science* **268**, 297–300.

Stuart, G., Schiller, J. & Sakmann, B. (1997*a*). Action potential initiation and propagation in rat neocortical pyramidal neurons. *Journal of Physiology* **505**, 617–632.

Stuart, G., Spruston, N., Sakmann, B. & Häusser, M. (1997*b*). Action potential initiation and backpropagation in neurons of the mammalian CNS. *Trends in Neurosciences* **20**, 125–131.

Stuart, G. J., Dodt, H. U. & Sakmann, B. (1993). Patch-clamp recordings from the soma and dendrites of neurons in brain slices using infrared video microscopy. *Pflügers Archiv* **423**, 511–518.

Stuart, G. J. & Sakmann, B. (1994). Active propagation of somatic action potentials into neocortical pyramidal cell dendrites. *Nature* **367**, 69–72.

Tsaur, M. L., Chou, C. C., Shih, Y. H. & Wang, H. L. (1997). Cloning, expression and CNS distribution of Kv4.3, an A-type K^+ channel α subunit. *FEBS Letters* **400**, 215–220.

Tsubokawa, H. & Ross, W. N. (1997). Muscarinic modulation of spike backpropagation in the apical dendrites of Hippocampal CA1 pyramidal neurons. *Journal of Neuroscience* **17**, 5782–5791.

Turner, R. W., Meyers, D. E., Richardson, T. L. & Barker, J. L. (1991). The site for initiation of action potential discharge over the somatodendritic axis of rat hippocampal CA1 pyramidal neurons. *Journal of Neuroscience* **11**, 2270–2280.

White, E. L. (1989). *Cortical Circuits*: *Synaptic Organisation of the Cerebral Cortex Structure, Function, and Theory.* Birkhauser, Boston.

Yuste, R. & Tank, D. W. (1996). Dendritic integration in mammalian neurons, a century after Cajal. *Neuron* **16**, 701–716.

Acknowledgements

The authors would like to thank M. Kaiser for superb technical help, Drs S. Bergling, D. Feldmeyer, K. M. M. Kaiser, M. E. Larkum, O. Ohana, A. Roth, S. D. Silberberg, W. Stühmer and Y. Zilberter for commenting on the manuscript. A.K. was a Minerva fellow.

Corresponding author

A. Korngreen: Abteilung Zellphysiologie, Max-Planck-Institut für Medizinische Forschung, Jahnstrasse 29, D-69120 Heidelberg, Germany.

Email: alon@mpimf-heidelberg.mpg.de